

Sustainable whey proteins-nanostructured zinc oxide-based films for the treatment of chronic wounds:
New insights from biopharmaceutical studies

Original

Sustainable whey proteins-nanostructured zinc oxide-based films for the treatment of chronic wounds: New insights from biopharmaceutical studies / Pino, Paolo; Vigani, Barbara; Valentino, Caterina; Ianev, Daiana; Ruggeri, Marco; Boselli, Cinzia; Cornaglia, Antonia Icaro; Grisoli, Pietro; Onida, Barbara; Bosco, Francesca; Sandri, Giuseppina; Rossi, Silvia. - In: INTERNATIONAL JOURNAL OF BIOLOGICAL MACROMOLECULES. - ISSN 0141-8130. - ELETTRONICO. - 263:(2024), pp. 1-11. [10.1016/j.ijbiomac.2024.130655]

Availability:

This version is available at: 11583/2987388 since: 2024-03-28T15:33:28Z

Publisher:

Elsevier

Published

DOI:10.1016/j.ijbiomac.2024.130655

Terms of use:

This article is made available under terms and conditions as specified in the corresponding bibliographic description in the repository

Publisher copyright

Elsevier postprint/Author's Accepted Manuscript

© 2024. This manuscript version is made available under the CC-BY-NC-ND 4.0 license
<http://creativecommons.org/licenses/by-nc-nd/4.0/>. The final authenticated version is available online at:
<http://dx.doi.org/10.1016/j.ijbiomac.2024.130655>

(Article begins on next page)

1 Sustainable Whey proteins-Nanostructured zinc
2 oxide-based films for the treatment of chronic
3 wounds: new insights from biopharmaceutical studies

4 *Paolo Pino^{1#}, Barbara Vigani^{2#}, Caterina Valentino², Daiana Ianev², Marco Ruggeri², Cinzia*
5 *Boselli², Antonia Icaro Cornaglia³, Pietro Grisoli², Barbara Onida^{1*}, Francesca Bosco¹,*
6 *Giuseppina Sandri², Silvia Rossi^{2*}*

7 ¹Department of Applied Science and Technology, Politecnico di Torino, 10129 Turin, Italy;

8 ²Department of Drug Sciences, University of Pavia, 27100 Pavia, Italy.

9 ³Department of Public Health Experimental and Forensic Medicine, University of Pavia, 27100
10 Pavia, Italy

11 # These authors equally contributed to the present work

12

13 **KEYWORDS:** bionanocomposite, whey proteins based films, antibacterial properties, cell
14 proliferation, wound healing

15 **ABSTRACT:** Chronic wounds represent silent epidemic affecting a large portion of the world
16 population, especially the elders; in this context, the development of advanced bioactive dressings
17 is imperative to accelerate wound healing process, while contrasting or preventing infections. The
18 aim of the present work was to provide a deep characterization of the functional and
19 biopharmaceutical properties of a sustainable thin and flexible films, composed of whey proteins
20 alone (WPI) and added with nanostructured zinc oxide (WPZ) and intended for the management

21 of chronic wounds. The potential of whey proteins-based films as wound dressings has been
22 confirmed by their wettability, hydration properties, elastic behavior upon hydration,
23 biodegradation propensity and, when added with nanostructured zinc oxide, antibacterial efficacy
24 against both Gram-positive and Gram-negative pathogens, i.e. *Staphylococcus aureus* and
25 *Escherichia coli*. *In-vitro* experiments, performed on normal human dermal fibroblasts, confirmed
26 film cytocompatibility, also revealing the possible role of Zn^{2+} ions in promoting fibroblast
27 proliferation. Finally, *in-vivo* studies on rat model confirmed film suitability to act as wound
28 dressing, since able to ensure a regular healing process while providing effective protection from
29 infections. In particular, both films WPI and WPZ are responsible for the formation in the wound
30 bed of a continuous collagen layer similar to that of healthy skin.

31 **1. INTRODUCTION**

32 Chronic wounds represent a major and often overlooked problem for healthcare [1]: in the last 5
33 years, chronic wounds have become a serious life-threatening disease, showing a comparable
34 mortality rate to cancer [2]. Several factors, especially metabolic disorders, aging, vascular
35 deficits, trauma and severe infectious disease (i.e. COVID-19), may worsen primary wounds,
36 prolonging their healing process [3, 4]; additionally, delayed wound management has been of
37 particular concern during the COVID-19 pandemic, increasing the risk of infections [5]. In most
38 cases, chronic wounds are exacerbated by the high exposure to infections, which are responsible
39 for worsening the patient's health and extending the duration of hospital stays. In an alarmingly
40 increasing number of cases, pathogenic bacteria are also found to be poorly sensitive to both
41 systemic and topical antimicrobial therapy because of widespread antibiotic resistance [6].

42 This scenario calls for urgent action, especially concerning the development of advanced
43 wound dressings capable of contrasting or preventing infections, while promoting healing [7,8].

44 To address the antibiotic resistance, the research on new antimicrobial agents has
45 demonstrated the potential of nanostructured materials, such as metal-oxide one [9,10].
46 Nanostructured zinc oxide (nZnO) is a promising nanomaterial with renowned antimicrobial,
47 antioxidant, and anti-inflammatory properties [11]. The release of Zn^{2+} ions represent the principal
48 mechanism of antimicrobial action of nZnO, as well as the production of reactive oxygen species
49 and the physical interactions with bacterial cells [12,13]. Moreover, zinc is an essential trace
50 element for the human body and takes an active part in wound healing, supporting re-
51 epithelialization and skin modelling [14]. All these properties make nZnO a particularly promising
52 filler for the preparation of biopolymer-matrix composite (defined as bionanocomposite), although
53 concerns still exist about the potential cytotoxicity of its nano-sized form [15, 16].

54 Whey proteins, particularly in the form of Whey Protein Isolate (WPI), are obtained from whey,
55 that is the most important by-product of the dairy industry: the disposal of a large amount of whey
56 as wastewater involves serious environmental hazards and represents a significant loss of potential
57 ingredients, such as lactose, fat and proteins. In an attempt to exploit the whey value and to mitigate
58 its harmful effects on the environment, it seemed useful to direct whey management towards a
59 sustainable way of utilization, such as the production of novel valuable products [17]. Whey
60 proteins represent a promising biomaterial known for its biodegradability and bioactivity [18]: It
61 contains high levels of amino acids, such as arginine, glycine, leucine, isoleucine and valine, which
62 are essential in the promotion of wound healing, and proline, that is considered pivotal for collagen
63 biosynthesis, structure and strength [19]. For thirty years now, whey proteins are known for their
64 excellent film-forming ability driven by the formation of hydrophobic interactions and
65 intermolecular disulfide bridges upon protein denaturation [20]. In particular, whey proteins have
66 recently gained attention in the food packaging industry: such biopolymers are involved in the
67 formation of edible films, endowed with outstanding mechanical (i.e. flexibility) and barrier

68 properties (i.e. high water vapor permeability and excellent oxygen permeability), which serve as
69 a functional food-environment barrier ensuring food safety and quality [21,22].

70 All these properties suggest that whey proteins could be used for the fabrication of
71 sustainable and innovative wound dressings; actually, there are no published studies on the use of
72 whey proteins-based films for wound healing applications. Nowadays, only an oral
73 supplementation with whey proteins has been proposed as an interesting strategy to integrate the
74 local treatment of wounds [23,24].

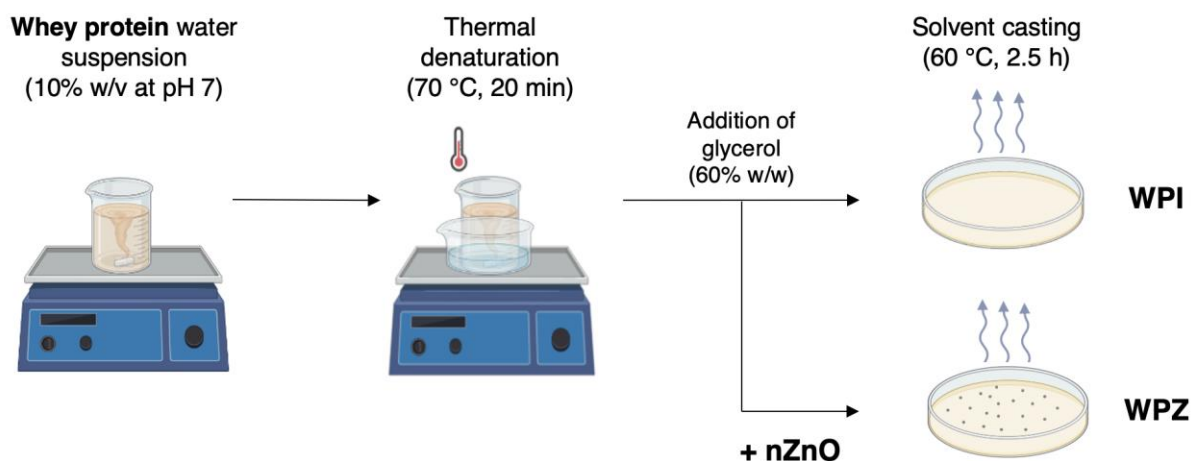
75 A previous work of ours demonstrated how whey proteins and nZnO can be combined by
76 a simple procedure to obtain flexible and antibacterial films based on WPI-nZnO
77 bionanocomposite for biomedical and food packaging applications [25]. The present work further
78 expands on this research by investigating some peculiar features of whey proteins-based films and
79 WPI-nZnO bionanocomposite-based films (i.e. film morphology, hydration propensity,
80 biodegradation behavior and antibacterial efficacy against *S. aureus* and *E. coli*), which could be
81 relevant for their use in wound healing application. In fact, to the best of our knowledge, it is the
82 first time that whey proteins-based films with and without nZnO were proposed as innovative
83 wound dressings and characterized for their biopharmaceutical properties both *in-vitro* and *in-vivo*.
84 Moreover, in the present work the *in-vitro* effects of the films on human dermal fibroblast viability
85 and proliferation are investigated, and an *in-vivo* test is ultimately carried out on a murine model
86 to prove their wound healing potential.

87 **2. MATERIALS AND METHODS**

88 **2.1. Materials.** Zinc acetate di-hydrate ($\geq 98\%$), potassium hydroxide ($\geq 85\%$), and absolute
89 ethanol were obtained from Sigma-Aldrich (St. Louis, MO, USA) and used as received. Whey
90 Protein Isolate (WPI) was kindly supplied by Milei GmbH (Leutkirch im Allgäu, Germany).

91 **2.2. Synthesis of nZnO.** nZnO was obtained from wet chemical precipitation as reported in [25].
92 Zinc acetate dihydrate (29.50 g) and potassium hydroxide (14.80 g) were dissolved in 120 mL and
93 64 mL of ethanol respectively, and subsequently mixed and kept at 60°C for 72 h under stirring
94 and reflux. The white precipitate was recovered by means of a 30 min centrifugation cycle at 1073
95 g (ALC PK1110 centrifuge; DJB Labcare Ltd, Newport Pagnell, England) and subsequently washed
96 three times with ethanol and dried overnight at 60°C.

97 **2.3. Preparation of whey proteins-based films (WPI films) and WPI-nZnO**
98 **bionanocomposite-based films (WPZ).** WPI and WPZ films have been prepared according to the
99 procedure previously described in [25] (Figure 1). Briefly, a 10% (w/w) WPI suspension was
100 prepared in distilled water and its pH was brought to 7.0 with dropwise addition of 1 M NaOH.
101 The suspension was heat-treated at 70°C for 20 min in a thermostatic bath under constant stirring
102 and subsequently cooled down in a water bath at room temperature. A glycerol amount equal to
103 60% (w/w) of the dry protein weight contained in the suspension was added as plasticizing agent.
104 The so-obtained film-forming solution was then casted onto non-stick molds maintaining a
105 volume-to-surface ratio equal to 0.135 m, and finally dried for 2.5 h at 60°C. This allowed to obtain
106 WPI films. For the preparation of WPZ films, a mass of nZnO equal to 4% (w/w) of the dry protein
107 weight was dispersed in distilled water and sonicated in an ultrasound bath for 1 h. The
108 nanoparticles suspension was then mixed with the heat-treated film-forming solution right after
109 the addition of glycerol, and the resulting mix was casted and dried.



110

111 **Figure 1.** Schematic representation of solvent-casting method for the preparation of WPI and
 112 WPZ films.

113 **2.4. Microstructural Analyses.** Morphological evaluation of WPI and WPZ films was
 114 performed by means of a scanning electron microscope (Phenom Pure G6 SEM, ThermoFisher
 115 Scientific, Waltham, MA, USA), equipped with LUXOR Gold-Coater. Different magnifications
 116 were considered for each film. Film topography and nZnO distribution into WPZ matrix were
 117 assessed by means of Atomic Force Microscopy (Tosca 200, Anton Paar, Graz, Austria) in tapping
 118 mode (cantilever AP-ARROW-NCR, Silicon SPM-Sensor, Al-coating; thickness: 4.6 μm , length:
 119 160 μm , width: 45 μm); tapping mode images were acquired with a resonance frequency equal to
 120 285 kHz and force constant of 42 N/m. The resulting data were transformed into a 3D image. The
 121 mean surface roughness (S_a) of WPI and WPZ films was also calculated.

122 **2.5. Water Contact Angle Measurements.** Water Contact Angle (WCA) was measured using
 123 a DMe-211 Plus Contact Angle Meter (Kyowa Interface Science Co Ltd., Saitama, Japan)
 124 according to the $\theta/2$ method. For the test, a drop (10 μL) of Phosphate Buffer Solution (PBS, pH
 125 7.4; Biosolve Chimie, Dieuze, France) was deposited onto the surface of WPI and WPZ samples

126 and the contact angle was measured over time at 1 s intervals using FAMAS Dropmaster Software.
127 The experiment was repeated five times.

128 **2.6. Hydration test.** A hydration test was carried out to monitor water uptake of the film over
129 time. An experimental set-up has been designed to simulate the contact conditions between the
130 films and an exuding wound area. The wells of a polypropylene plate (Corning® 12 Well TC-
131 Treated Microplates, New York, NY, USA) have been filled to the brim with PBS. Subsequently,
132 a sheet of Parafilm® has been applied over the plate and pierced in correspondence of the PBS-
133 filled wells, allowing the liquid to emerge and to form a wet layer on the Parafilm®. WPI and WPZ
134 films have been cut in circular specimens with the same diameter of the wells, dried in an oven at
135 60°C until stabilization of the weight, and applied on top of an equally shaped dialysis membrane.
136 The experimental set-up used for the hydration test allowed to safely manipulate the films across
137 the entire duration of the experiment without compromising their integrity. Membrane-supported
138 film specimens have thus been placed on the wet Parafilm®, and the entire set-up was placed inside
139 an incubator at 32°C to simulate the temperature of the skin. To measure the swelling ratio (SR),
140 specimens were collected, blotted away of excess water with a filter paper, and weighted. The SR
141 was then determined according to the following equation:

$$142 \quad SR = \frac{m_w - m_d}{m_d} \times 100$$

143 where m_w is the wet mass and m_d is the dry initial mass. The swelling ratio has been calculated
144 after 1, 3, 6 and 24 h. The experiment has been done in triplicate.

145 **2.7. Viscoelastic Properties after Hydration.** After 24 h hydration, dynamic oscillatory
146 measurements were performed by means of a rotational rheometer (MCR102, Anton Paar, Turin,
147 Italy), using a parallel plate combination (PP25, diameter = 25 mm) as measuring system. Stress
148 sweep test was performed at 1 Hz frequency to identify the linear viscoelastic region (LVR). In
149 the oscillation test, a shear stress equal to 1 Pa (within the LVR previously determined) was applied

150 at increasing frequencies (1 to 10 Hz) and G' (storage modulus) and G'' (loss modulus) profiles
151 were recorded; measurements were performed at 32°C. Three replicates were considered for each
152 sample.

153 **2.8. Degradation test.** The degradation profile of WPI and WPZ films was investigated by
154 soaking the samples in two different degradation media: PBS [26] and H_2O_2 500 μ M in PBS [27].
155 In detail, WPI and WPZ circular specimens have been dried at 60°C until stabilization of the
156 weight (30 ± 5 mg) and subsequently immersed in 5 mL of PBS or H_2O_2 500 μ M in PBS. Immersed
157 films have been kept at 32°C for the duration of the entire experiment.

158 After 1, 3 and 7 days, sample degradation was evaluated in terms of (i) film residual mass and
159 (ii) protein concentration dissolved in the degradation media.

160 In particular, films have been collected and dried in an oven at 60°C until stabilization of the
161 weight. The percentage of residual mass (R) has been determined as:

$$162 \quad R = \frac{m_0}{m_f} \times 100$$

163 where m_f is the final residual dry mass and m_0 is the dry initial mass. The experiment has been
164 repeated three times.

165 Thereafter, the amount of protein fraction dissolved in each medium as a consequence of film
166 degradation was determined by means of UV-Vis spectroscopy analysis (spectrophotometer UV-
167 vis Lambda 25, Perkin Elmer, Milan, Italy) at $\lambda = 280$ nm; this method is particularly useful and
168 offers high specificity for proteins that contain tryptophan or tyrosine residues such as whey
169 proteins [28].

170 A calibration curve was used to determine the protein concentration in the medium after film
171 degradation: solutions containing increasing concentrations (from 0.001 to 1 mg/ml) of
172 denaturated WPI were prepared. Three replicates were considered for each sample.

173 **2.9. Antimicrobial test.** The antibacterial activity of WPI and WPZ films was investigated
174 against *Staphylococcus aureus* ATCC 6538 (Gram-positive) and *Escherichia coli* ATCC 10356
175 (Gram-negative). Before testing, the microorganisms were grown overnight in Tryptone Soya
176 Broth (Oxoid; Basingstoke, Hampshire, England) at 37°C. Washed cells were resuspended in
177 Dulbecco's PBS and optical density (OD) was adjusted to 0.3, corresponding approximately to
178 110^8 Colony Forming Units (CFU/ml) at 650 nm wavelength.

179 Ten μ l of bacterial suspension was placed on a standard glass slide (76 \times 26 mm); the microbial
180 suspension was, then, covered with WPZ film (20 \times 20 mm), forming a thin film that facilitates
181 direct contact of the microorganisms with the active WPZ surface. The assembled glasses were
182 introduced in a Falcon test-tube (50 ml) containing 1 ml of PBS to maintain a damp environment;
183 the WPZ surfaces were maintained in contact with the liquid films containing bacteria at room
184 temperature for 6 and 24 hours; for each time of contact, WPI film was treated in the same way,
185 as control sample. After the times of contact, 9 ml of PBS were introduced in each Falcon test-
186 tube under a gentle shaking to detach the glass slides from WPZ and WPI surfaces. Bacterial
187 suspensions were then grown in Tryptone Soya Agar to count viable cells. The decimal-log
188 reduction rate, microbicidal effect (ME), was calculated using the following equation:

$$189 \quad \text{ME} = \log \text{NC} - \log \text{NE}$$

190 where NC is the number of CFU/ml developed on the control glasses (WPI film), whereas NE
191 is the number of CFU/ml counted after exposure to WPZ surfaces. The results expressed as ME
192 represent the average of three equivalent determinations [29,30].

193 **2.10. *In-vitro* cytocompatibility test.** Normal Human Dermal Fibroblasts (NHDF) from
194 juvenile foreskin (PromoCell GmbH, VWR, Milan, Italy) from 6th to 12th passage were used. Cells
195 were cultured in polystyrene flasks in Dulbecco's Modified Eagle's Medium (DMEM),
196 supplemented with 10% v/v heat-inactivated Foetal Bovine Serum (FBS) (VWR International

197 S.r.l, Milan, Italy), and with 1% v/v antibiotic-antimycotic solution (Merk Life Science S.r.l.,
198 Milan, Italy), at 37°C in 5% CO₂ atmosphere.

199 Extraction dilution method was performed to investigate the cytotoxic effect of WPI and WPZ
200 films [31]. More in detail, WPI and WPZ specimens (0.32 cm²), previously sterilized through UV
201 irradiation, were soaked in 600 µL of complete culture medium (CM) for 24 h at 37°C for obtaining
202 film extracts; then, the extracts were collected and serially diluted (1:2, 1:10, 1:50, 1:100 v/v) by
203 adding fresh CM.

204 Fibroblasts was seeded at a density of 1.0×10^5 cells/well into a 96-well plate and incubated
205 (37°C and 5% CO₂) for 24 h in order to reach semi-confluence. After the medium had been
206 replaced with the extracts, as such or diluted, the cells were incubated for a further 24 h; CM was
207 used as a reference. After incubation, an MTT assay was performed. Briefly, extracts and reference
208 were removed from the 96-well plate and cell monolayers were washed with Phosphate Buffer
209 Solution (PBS); subsequently, 50 µl of MTT 7.5 µM in 100 µl of DMEM without phenol red were
210 added to each well and incubated for 3 h (37°C and 5% CO₂). Finally, 100 µl of DMSO was added
211 to each well in order to promote the complete dissolution of formazan crystals, obtained from MTT
212 dye reduction by mitochondrial dehydrogenases of living cells. The solution absorbance was
213 measured by means of an iMark® Microplate reader (Bio-Rad Laboratories S.r.l.) at a wavelength
214 of 570 nm and 690 nm (reference wavelength) after 60 s of mild shaking. Six replicates were
215 considered for each sample.

216 **2.11. *In-vitro* proliferation test.** The extracts, obtained as previously described at 24 h, were
217 also investigated for their capability to enhance NHDF proliferation at 1, 3 and 7 days. Cells were
218 seeded into a 96-well plate at a density of 2.0×10^4 cells/50 µL of CM/well and immediately added
219 with 150 µL extracts diluted 1:2 v/v with fresh CM. CM was used as a reference. Finally, an MTT
220 test was performed as described in the previous paragraph. Six replicates were considered for each

221 sample. Results were expressed as cell viability % by normalizing the absorbance measured after
222 contact with each sample with that measured for CM, used as reference. Six replicates were
223 performed for each sample/control.

224 **2.12. *In-vivo* studies**

225 **2.12.1 Evaluation of wound healing-enhancing properties on rat model.** All animal
226 experiments were carried out as previously described [32] in full compliance with standard
227 international ethical guidelines (European Parliament 2013) (European Communities Council
228 Directive 86/609/EEC) approved by the Italian Health Ministry (Italian Health Ministry 2021).
229 The study protocol was approved by the Local Institutional Ethics Committee of the University of
230 Pavia for the use of animals.

231 In brief, male rats (Wistar 200–250 g) (n=4) were anesthetized with equitensine (3 mL/kg) and
232 shaved to remove all hair from the site of injury. Three full-thickness burns were produced on the
233 animal's back by contact with a brass rod (105°C for 40 s), having a circular diameter of 4 mm.
234 After 24 h, three 6-mm full-thickness excisional wounds were outlined using a punch biopsy tool
235 on each animal back. Wounds were photographed with a digital camera and then treated with i)
236 WPI film (0.32 cm²) moistened with 25 µL of saline (NaCl 0.9% w/v), ii) WPZ film (0.32 cm²)
237 moistened with 25 µL of saline and iii) 25 µL of saline as control. Subsequently, each wound was
238 covered with a sterile gauze and the rat's back was wrapped with a surgery stretch (Safety, Monza,
239 Italy), to keep films or the physiological solution into the wound bed. At prefixed times after
240 treatment (3, 7, 14, and 18 days), the three lesions were photographed with a digital camera in
241 order to monitor wound healing process. The wound healing potential of WPI and WPZ films was
242 evaluated by wound area retraction (%) using the following equation:

$$243 \text{ Wound area retraction (\%)} = (A_t/A_0) \times 100$$

244 where A_0 is the initial wound area and A_t is the wound area at different time points; the wound
245 area was determined using the imaging analysis program ImageJ 2.0.

246 **2.12.2 Histological analysis.** After 18-day treatment, the animals were sacrificed. After
247 euthanasia, the area around the scar or residual wound was harvested and wound tissue specimens
248 (wound bed) were immediately immersed in the fixative solution (4% neutral buffered
249 formaldehyde), embedded in paraffin and sectioned at a thickness of 5 μm . Some sections were
250 stained with hematoxylin and eosin (H&E), others with picosirius red (PSR).

251 Picosirius polarization method is one of the best understood techniques of collagen
252 histochemistry and it is particularly useful to reveal the organization and the heterogeneity of
253 collagen fiber in different connective tissues. Polarizing light assessment of PSR stain identified
254 the old thick collagen I fibers as orange-to-red and the newly deposited, rich in collagen III fibers,
255 as green [33,34]. Picosirius red stain was applied as follows: deparaffinized sections were
256 hydrated, faintly stained with Weigert's hematoxylin for nuclei and stained with PSR (1 hour).
257 Then all sections were dehydrated, cleared in xylene and mounted with DPX (dibutyl phthalate in
258 xylene).

259 Stained slices were observed with a light microscope Carl Zeiss Axiophot (Oberkochen,
260 Germany) provided, for circular polarizing microscopy, with suitable filters in the condenser stage
261 and in the microscope tube. Images were recorded through a microscope digital 5 megapixels CCD
262 camera Nikon DS - Fi2.

263 **2.12. Statistical analysis.** Whenever possible, experimental data were subjected to statistical
264 analysis, carried out by means of the statistical package Statgraphics 5.0 (Statistical Graphics
265 Corporation, Rockville, Maryland, USA). In particular, one-way ANOVA was carried out
266 followed by a Multiple Range Test.

267 **3. RESULTS AND DISCUSSION**

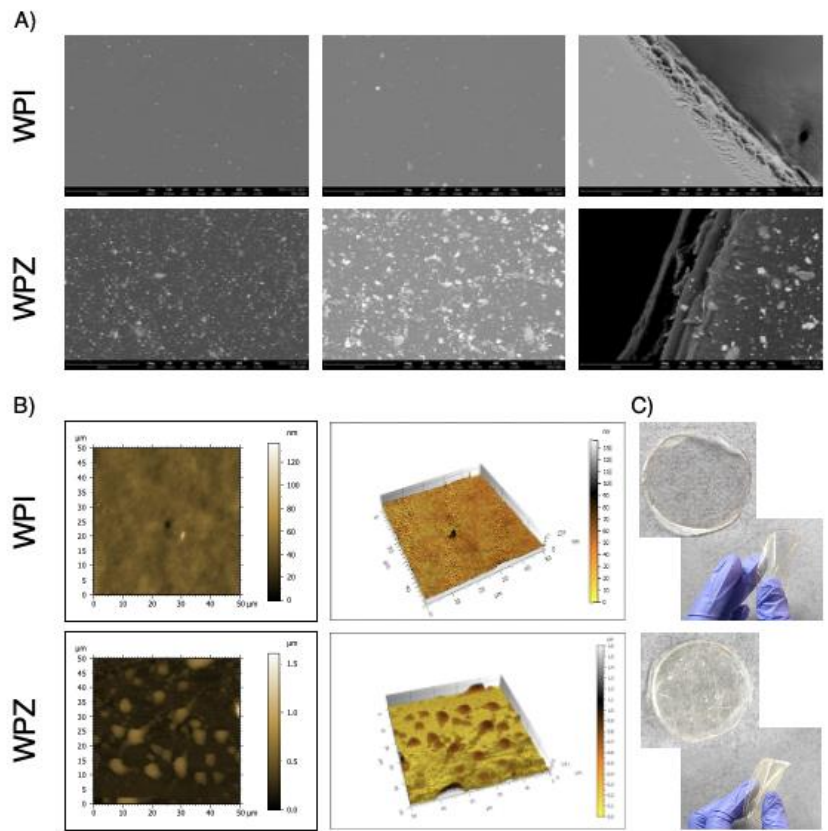
268 Whey Protein Isolate-based films, endowed with optimal barrier properties and the capability to
269 load various functional agents (i.e. antimicrobials and prebiotics/probiotics), have increasingly
270 attracted the attention of the scientific community, sometimes outperforming polysaccharide- and
271 other protein-based films [22]. In recent years, the use of biopolymers, obtained from renewable
272 sources or industrial by-products, in the manufacturing of flexible and edible films for food
273 packaging has proved to be an environmentally friendly and sustainable strategy to replace
274 petroleum-based packaging materials [35]. Besides the well-known whey proteins nutritional
275 value, the numerous health benefits of WPI encourage researchers to develop new WPI-based
276 therapeutic platforms intended for different biomedical purposes [18, 36]. In particular, WPI
277 appears to be a valuable candidate for the production of dressings for wound healing applications
278 [37]. It contains a high level of amino acids, both essential and non-essential ones, which are
279 involved in protein synthesis, and it is a rich source of glutamine required to support cellular
280 growth and proliferation [38]. Moreover, the addition of nZnO into WPI-based films, as proposed
281 in our previous work [25], could appear useful for treating skin wounds; in fact, it is reported in
282 the literature that ZnO nanoparticles have been successfully used in wound dressings thanks to
283 their strong antimicrobial properties following cutaneous application and their epithelialization-
284 stimulating effect [11,39].

285 In the present work, a biopharmaceutical characterization of the developed WPI and WPI-nZnO
286 bionanocomposite-based films was performed both *in vitro* and *in vivo* to investigate film
287 properties that are relevant for clinical applications in wound healing.

288 **3.1. Microstructural morphology and surface topography**

289 Figure 2A reports SEM micrographs of WPI and WPZ films. WPI film was characterized by a
290 smooth, compact and homogeneous surface, as opposed to WPZ bionanocomposite film that
291 showed a rough surface with evenly distributed nZnO (average particle size equal to 32 nm and

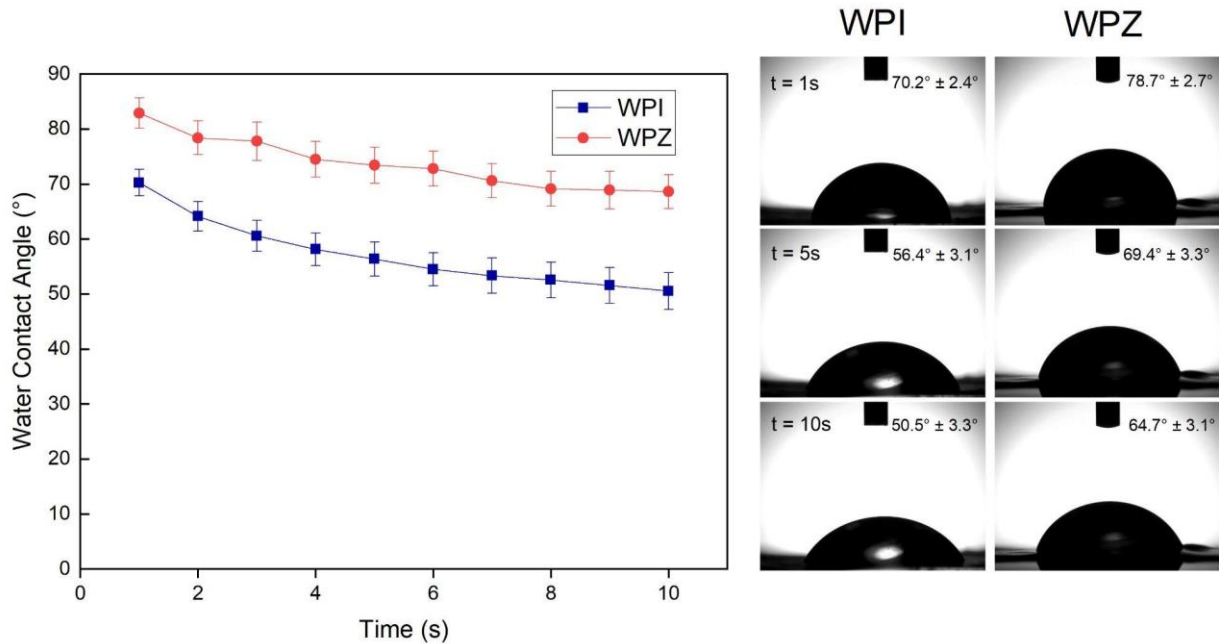
292 specific surface area of approximately $47.3 \text{ m}^2/\text{g}$). SEM micrographs highlight the presence of
 293 some aggregates of nZnO, which appear as shiny spots within WPZ film structure [40]. The
 294 formation of irregular nZnO aggregates is probably due to the high nanoparticle surface energy
 295 and occurs during solvent evaporation [25, 41, 42]. The topography of film surface was also
 296 investigated by AFM and results, as 2D and 3D images, are also shown in Figure 2B. Some
 297 aggregation of nZnO is responsible for an increase in roughness with the creation of deep valleys
 298 and high peaks; these results confirm SEM microstructural observations. S_a expresses, as an
 299 absolute value, the difference in height of each point compared to the arithmetical mean of the
 300 surface and, thus, is generally used to quantitatively define the surface roughness. S_a was 3.40 nm
 301 for WPI film and 79.4 nm for WPZ film, proving the presence of nZnO within biopolymer-based
 302 structure. Figure 2C shows the macroscopic appearance of WPI and WPZ films, endowed with an
 303 optimal flexibility and, thus, suitable for topical application on skin wounds.



304

305 **Figure 2.** SEM micrographs (A) and 2D and 3D AFM images (B) of WPI and WPZ films. C)
306 Macroscopic appearance of WPI and WPZ films.

307 **3.1. Water Contact Angle.** The surface wettability of whey proteins-based films, in presence
308 and in absence of nZnO, was evaluated by means of water contact angle (WCA) analysis. The
309 results of the WCA measurements are shown in Figure 3.

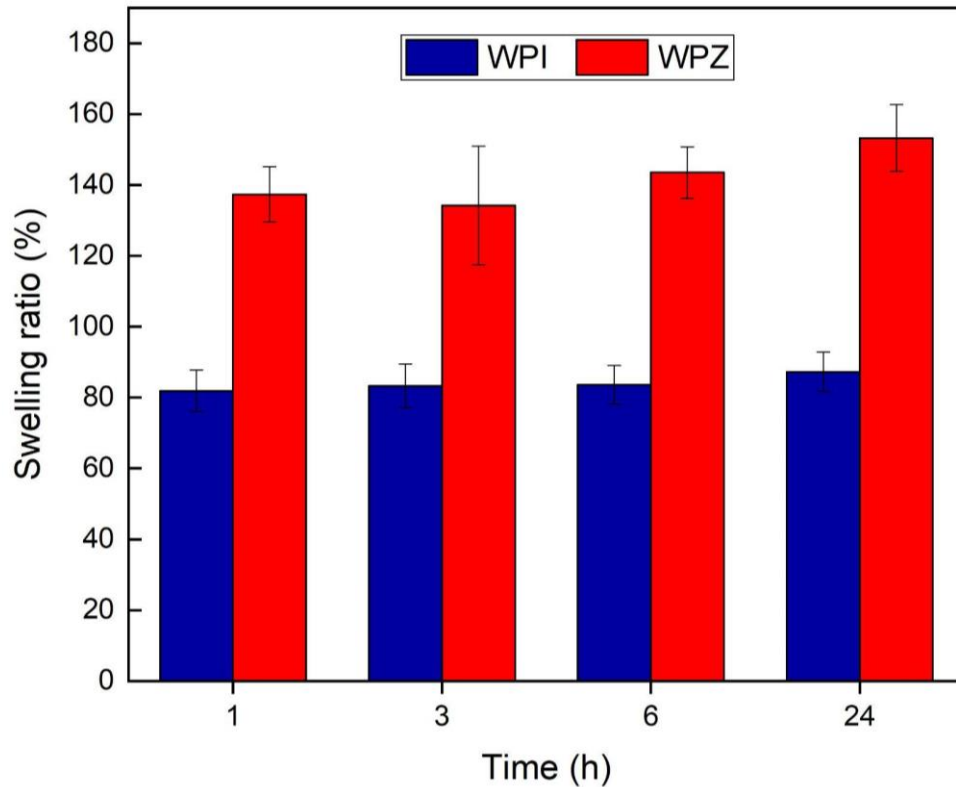


310
311 **Figure 3.** WCA values of WPI and WPZ films up to 10 s (mean values ± S.D.; n = 3). Images of
312 the drop at different times (1, 5, and 10 s) are reported for WPI and WPZ films.

313 As shown by the WCA values lower than 90°, both samples are hydrophilic. The addition of
314 nZnO causes a significant increase in WCA values (p-value < 0.05) in the time interval under
315 investigation. Such behavior is frequently observed for other biopolymer/nZnO nanocomposites
316 described in the literature [39, 43-45]. The reduced wettability of WPZ film can be related to both
317 the hydrophobic nature of nZnO incorporated into the biopolymer-based film and the increase in
318 WPZ surface roughness, appreciated in SEM and AFM images (Figure 2); in fact, it is well-known
319 that roughness makes hydrophobic surfaces more hydrophobic [46].

320 Moreover, Figure 3 shows that the value of WCA decreases over time in both samples. Thanks
321 to the overall good water affinity of the bionanocomposite, the droplet tends to spread across the
322 surface of the films, thus determining a decrease of WCA. After 10 s, the surface of both samples
323 starts deforming due to the absorption of the liquid droplet, which prevents longer-duration
324 measurements of the contact angle. WPI films were characterized by an initial WCA value equal
325 to $70.2^\circ \pm 2.4^\circ$ that decreases to $50.5^\circ \pm 3.3^\circ$ after 10 s. In WPZ film, WCA has an initial value of
326 $78.7^\circ \pm 2.7^\circ$, which goes down to $64.7^\circ \pm 3.1^\circ$ after 10 s. The results obtained are in line with the
327 literature since, generally, an ideal wound dressing is characterized by WCA value in the range of
328 $50-70^\circ$. Hydrophilicity is obviously a fundamental property for primary dressings, i.e., those
329 dressings that are placed in direct contact with the wound, in order to ensure exudate absorption
330 and good adhesion to the site. Hydrophilic dressings ensure support and protection to the wound,
331 reducing possible complications and accelerating the healing process [47,48].

332 **3.2 Hydration test.** The swelling ratio (SR) values were calculated for WPI and WPZ films
333 upon 24 h (Figure 4), allowing a quantitative evaluation of the ability of the film to absorb a
334 medium-simulating wound exudate (PBS) over time.



335

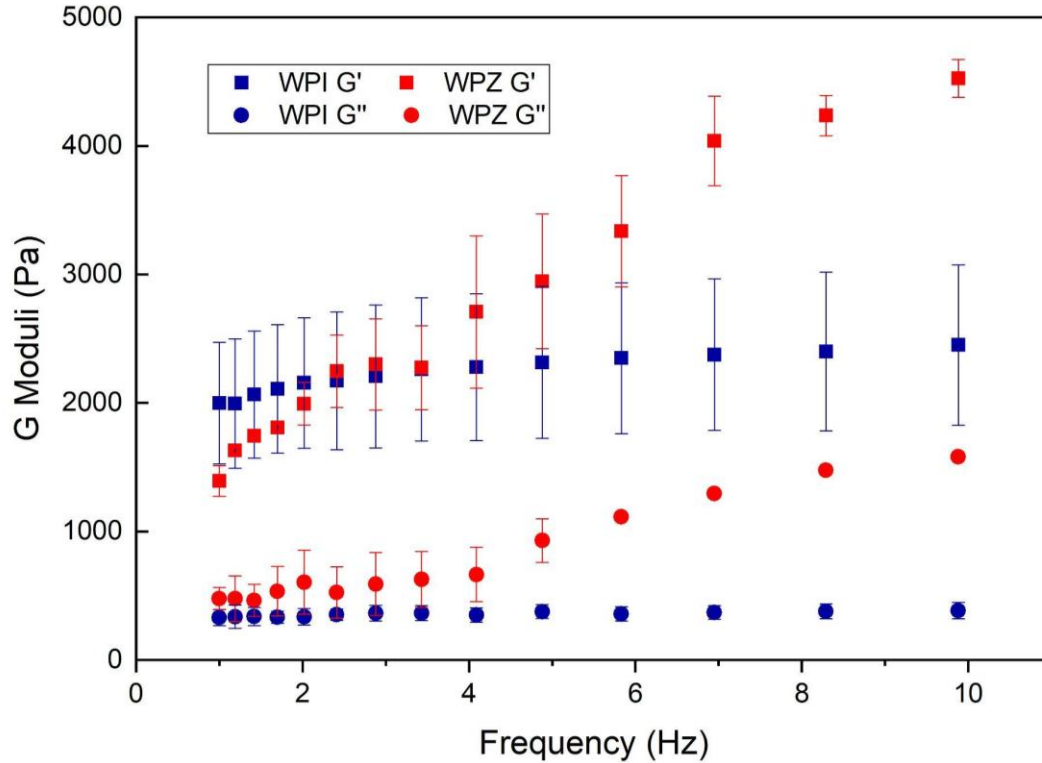
336 **Figure 4.** Variation in time of the swelling ratio % of WPI and WPZ films (mean values \pm S.D.; n
 337 = 6).

338 It can be noticed that WPZ samples showed higher (more than 1.5 times) SR values than WPI
 339 films. This is in agreement with previous studies [25] as well as with other scientific reports [48-
 340 50]. The increased SR value is attributed to the electrostatically charged surface of nZnO, which
 341 attracts ions in the PBS inducing a build-up of osmotic pressure inside the WPI matrix, in tum
 342 causing a higher PBS uptake.

343 Fluid uptake capability is an important parameter to be investigated for elucidating the film
 344 behavior after application at the injury site [26]. Indeed, a wound dressing should preserve a moist
 345 wound environment without enabling the accumulation of exudate, which could impair the healing
 346 process and be responsible for the maceration of the healthy surrounding tissue [51,52]. Generally,
 347 an ideal wound dressing must be characterized by SR values ranging between 100-900% [51,52].

348 Water uptake is rapid and occurs within the first 30 minutes, and then remains relatively stable
349 or slightly increasing throughout the whole experiment. For WPI films, SR is $81.88\% \pm 5.85\%$
350 after the first hour and becomes $87.25\% \pm 5.52\%$ after 24 h. In WPZ, SR has an initial value of
351 $137.36\% \pm 7.83\%$, which goes up to $153.26\% \pm 9.38\%$ after 24 h. This is an important feature for
352 wound dressings, as it demonstrates film stability for a prolonged time. It is worth noting that the
353 observed SR values are within the range reported in the literature as optimal [53,54].

354 **3.3 Viscoelastic Properties after Hydration.** The amount of PBS absorbed by both films
355 reached an equilibrium without compromising the film structural integrity. After 24 h of hydration,
356 WPI and WPZ films were subjected to viscoelastic measurements. As shown in Figure 5, both
357 samples were characterized by higher G' (storage elastic modulus) values than G'' (loss viscous
358 modulus) ones in the whole range of frequencies considered. Such behavior is highly desirable for
359 a wound dressing: once hydrated, both films, endowed with marked elastic properties compared
360 to viscous ones, are able to recover the deformation caused by external shear stresses and, thus, to
361 effectively protect the injured area [51,55]. The presence of nZnO is responsible for higher G' and
362 G'' values, in particular for frequencies higher than 7 Hz. Moreover, it can be observed that in
363 presence of nZnO both G' and G'' are characterized by a higher dependence on frequency; this
364 could be due to the fact that the inclusion of nZnO may disturb the WPI chain network, restricting
365 polymer chain mobility and, thus, resulting in an enhancement of elasticity [56].



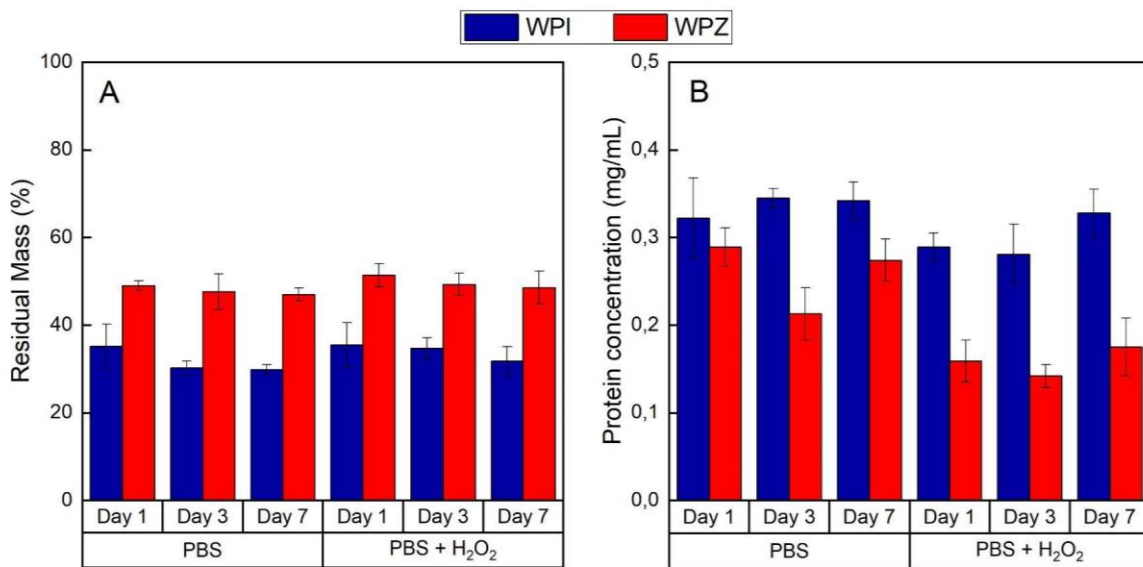
366

367 **Figure 5.** Storage (G') and loss (G'') moduli vs. frequency profiles of WPI and WPZ films upon
 368 24 h-hydration in PBS (mean values \pm S.D.; $n = 3$).

369 **3.4 Degradation test.** The degradation rates of WPI and WPZ films over 7 days are shown in
 370 Figure 6. After 1, 3 and 7 days, sample degradation was evaluated in terms of (i) film residual
 371 mass (Figure 6A) and (ii) protein concentration dissolved in the degradation media (Figure 6B).
 372 Two different degradation media were considered: PBS (pH = 7.4), mimicking wound exudate,
 373 and PBS added with H_2O_2 to simulate the oxidative stress in the early inflammatory phase of the
 374 healing process [57,58].

375 The majority of the degradation occurs within the first day, while the further permanence of the
 376 samples in the medium (until 7 days) produced no significant additional mass loss (Figure 6A). It
 377 can therefore be hypothesized that the large mass loss occurring at the beginning is linked to the
 378 out-diffusion of weakly bonded molecules, such as glycerol, which are commonly present in WPI,
 379 as well as proteins that have not taken part in the formation of the film. After 7 days, what remains

380 is the robust intermolecular network composed of WPI proteins held together by more hydrophobic
 381 interactions and disulfide bridges [59]. The addition of H₂O₂ to PBS did not accelerate the
 382 degradation process, suggesting that both WPI and WPZ films are resistant to these oxidative
 383 conditions. These results are reflected by the protein concentration assessed in the degradation
 384 media, where higher protein content is observed in correspondence of those samples where lower
 385 residual mass was reported (Figure 6B).



386
 387 **Figure 6.** WPI and WPZ film degradation after 1, 3 and 7 days in two different media - PBS and
 388 PBS added with H₂O₂ - expressed in terms of (A) residual film mass and (B) concentration of
 389 proteins released in the medium (mean values ± S.E.; n = 3).

390 In order to increase film degradation time, the combination of proteins with polysaccharides
 391 might be a promising, thanks to the interactions between the two molecules [60].

392 As far as the effect of nZnO on the film stability is concerned, a few considerations can be made.
 393 The excess of residual mass measured for WPZ samples with respect to WPI ones (Figure 6A)
 394 appears systematically higher than the mass of nZnO alone in the samples, which would be equal
 395 to 4% of the dry mass in the conservative assumption that all the nZnO was retained inside the

396 matrix during degradation. These results strongly suggest that the presence of nZnO somehow
397 limits the degradation of the film. This can be explained considering that nZnO stabilizes the
398 matrix through its interactions with the whey proteins, preventing or slowing down their diffusion
399 and dissolution in the medium [44, 61,62].

400 **3.5 Antimicrobial test.** The microbicidal effect (ME) of WPZ was evaluated on two different
401 bacterial strains (*S. aureus* and *E. coli*); WPI film was used as a control reference. For both the
402 microorganisms considered, WPZ film showed a microbicidal effect higher than WPI film; in
403 particular, a marked antimicrobial effect of WPZ film was observed on *E. coli*.

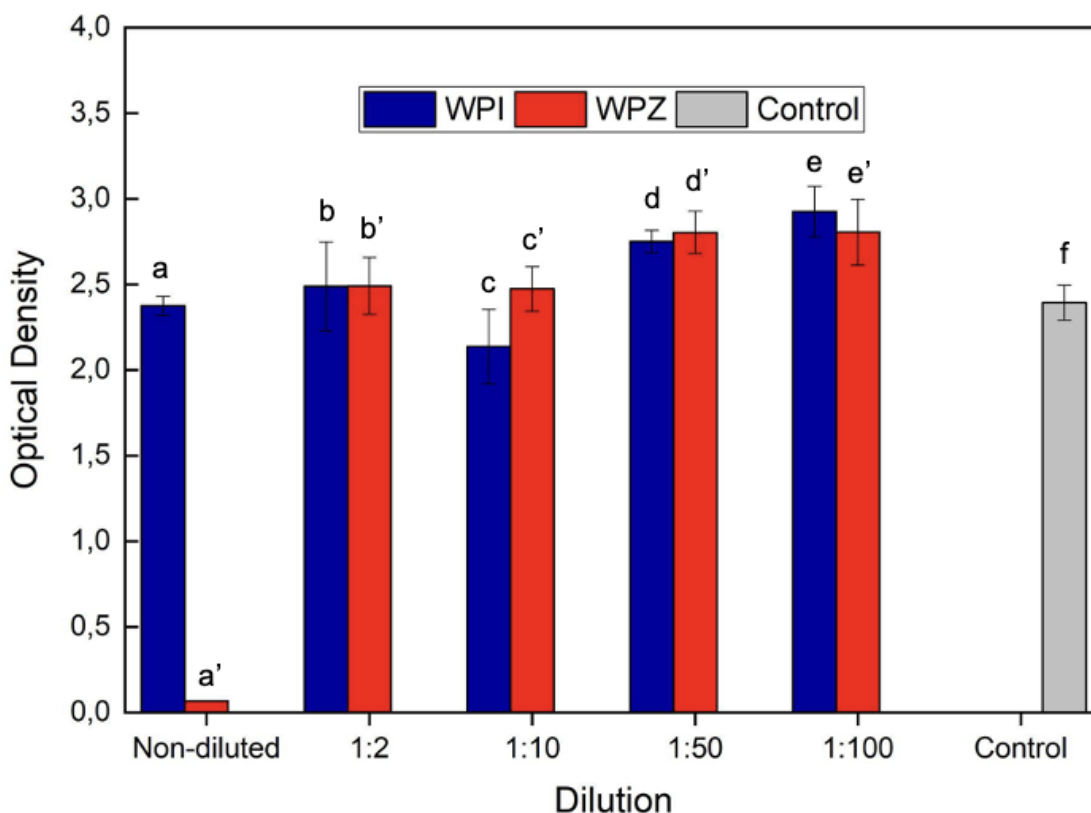
404 **Table 1.** Microbicidal effect (ME) of WPZ after 6 and 24 h incubation with *S. aureus* and *E. coli*;
405 WPI was used as control (CV % < 12%; n = 3).

	6 hours	24 hours
<i>S. aureus</i>	0.67	1.30
<i>E. coli</i>	2.85	4.94

406
407 These results reported in Table 1 confirm the well-known antibacterial properties of nZnO, but
408 some interesting pieces of evidence emerge. In particular, a stronger effect against the Gram-
409 negative was observed. The greater resistance of the Gram-positive to nZnO was attributable to
410 their thicker peptidoglycan layer [12].

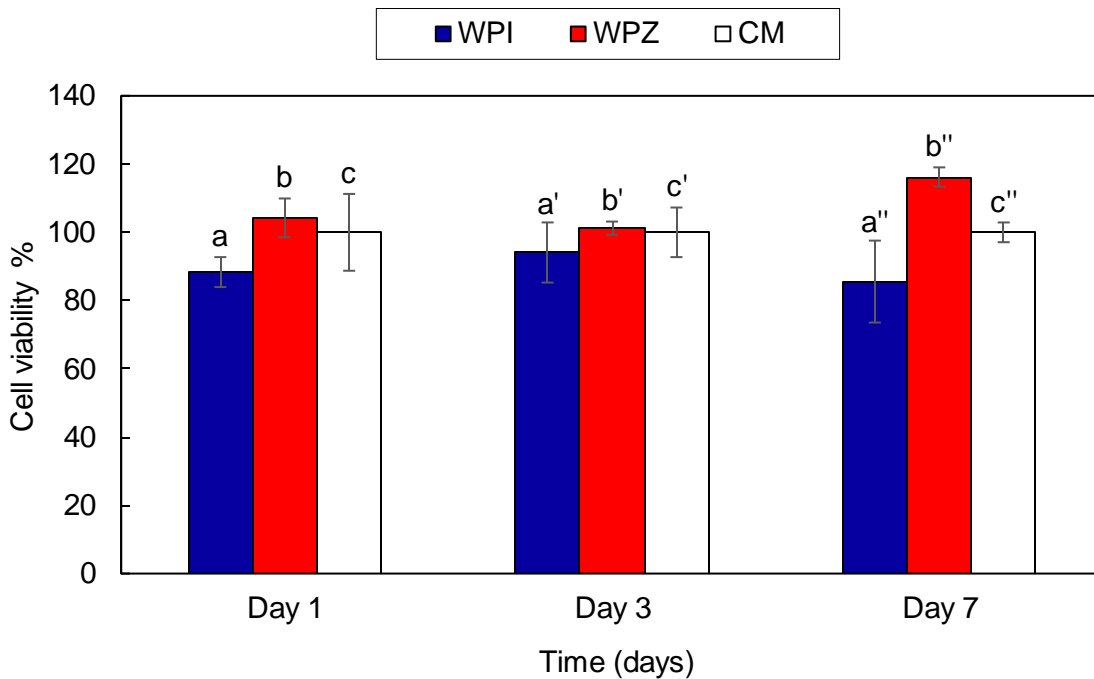
411 **3.6 In-vitro cytocompatibility test.** Film cytocompatibility was investigated by treating cells
412 with the media in which WPI or WPZ films were soaked for 24 h at 37°C; such media were called
413 film extracts. The results of the MTT assay carried on NHDF cells after 24 h incubation with film
414 extracts are shown in Figure 7. All the film extracts were cytocompatible except for the non-diluted
415 WPZ extract, as shown by the absorbance values reported in the graph. A very high concentration

416 of nZnO in the medium might in fact be detrimental for cells, as pointed out in several studies that
 417 raised concerns about the toxicity of metal oxide nanoparticles [63]. For ZnO nanoparticles, the
 418 release of Zn²⁺ ions has been considered the main toxicity mechanism on mammal cells, followed
 419 by the oxidative stress exerted by reactive oxygen species [15, 63]. However, cell viability is
 420 immediately restored with a 1:2 dilution and is preserved for all the subsequent dilutions. In fact,
 421 while toxic effects might arise at high concentrations, optimal amounts might allow to leverage
 422 the positive impact of zinc on the immune system and wound healing [11, 64, 65].



423
 424 **Figure 7.** Optical density values after 24 h incubation of NHDF cells with WPI and WPZ extracts,
 425 undiluted and diluted 1:2, 1:10, 1:50, 1:100 v/v in CM. Complete culture medium (CM) was
 426 considered as control (mean values \pm S.E.; n = 6). ANOVA one-way – Multiple Range Test (p-
 427 value \leq 0.05): a vs a', e; c vs d, e; e vs f; a' vs b', c', d', e', f.

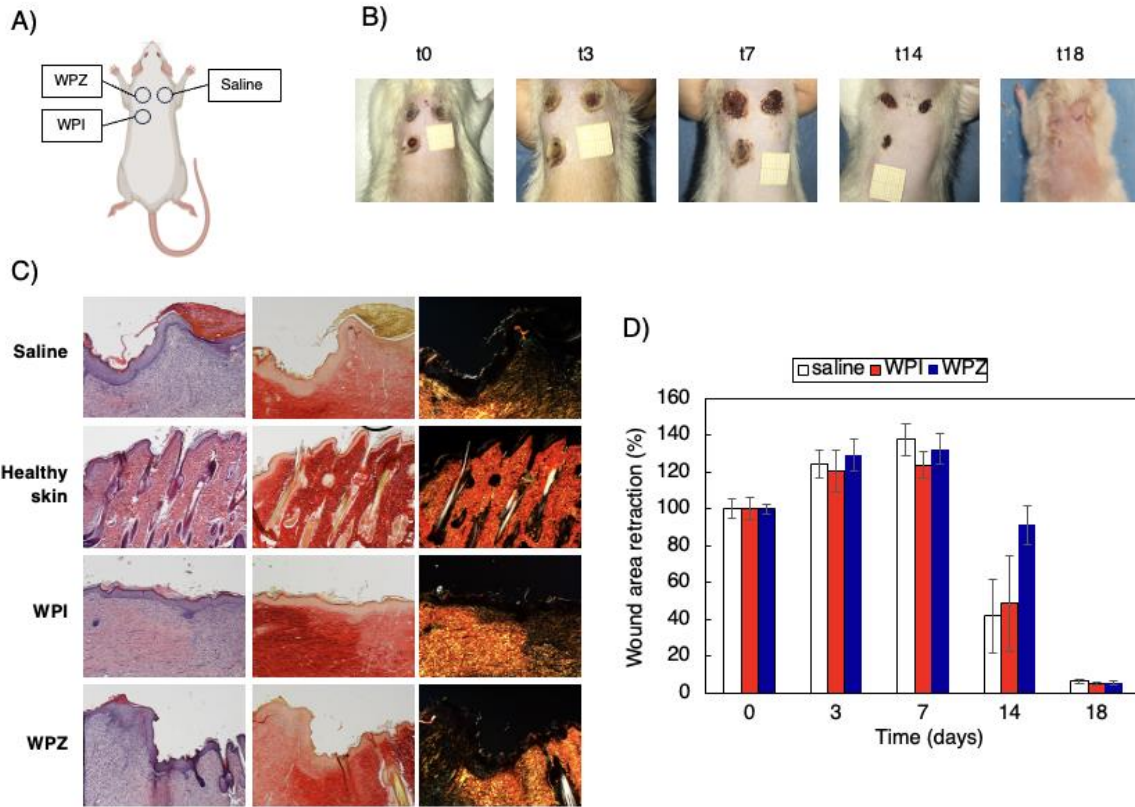
428 **3.7 *In-vitro* proliferation test.** Figure 8 shows the results of the MTT test performed after the
 429 *in-vitro* proliferation test carried on NHDF cells seeded using WPI and WPZ extracts, obtained
 430 after 1, 3 and 7 days and diluted 1:2 v/v in CM, as culture medium. WPZ induced a significantly
 431 higher proliferation compared to WPI and the control after 7 days of culture. This result, in
 432 accordance with the experimental evidence shown above (Figure 7), reveals the possible role of
 433 Zn^{2+} ions in fibroblast proliferation [14].



434
 435 **Figure 8.** Viability % values after 1, 3 and 7 days of proliferation of NHDF cells in WPI and WPZ
 436 extracts, diluted 1:2 v/v in CM. Complete culture medium (CM) was considered as control (mean
 437 values \pm S.E.; n = 6). ANOVA one-way – Multiple Range Test (p-value \leq 0.05): a vs b; a'' vs b'';
 438 b'' vs c''; b vs b''; b' vs b''.

439 **3.8 *In-vivo* wound healing test.** As it can be seen in Figure 9C, WPI and WPZ treated wounds
 440 show signs of the proliferative phase of healing, with a number of blood vessels and a residual area
 441 of granulation tissue (a mixture of proliferating capillaries, fibroblast and inflammatory cells in a

442 loose edematous extracellular matrix). The entire surface of the lesion treated with the films was
443 covered with new epithelium, fully restored in multiple layers of cells and with a fair degree of
444 keratinization. Skin appendages such as hair follicles and glands were reforming. According to
445 PSR staining, collagen was laid down and remodeled in an appropriate orientation to withstand
446 the tensile stresses placed on the area of repair, suggesting a maturation and remodeling phase of
447 the healing process [37,38,66]. A continuous collagen layer, rich in orange-to-red fibers, with a
448 pattern similar to that of healthy skin, can be observed for WPI and WPZ treated wounds. Figure
449 9C highlights that the regeneration process is accelerated in wounds treated with whey proteins-
450 based films with respect to saline. These results indicate that both WPI and WPZ films can be used
451 as effective wound dressing nonetheless, as they ensure a regular healing process while providing
452 effective protection from infections. After 18-day treatment, wound closure with completely
453 regenerated epithelium was assessed in each sample (Figure 9B and D). No WPI or WPZ films
454 nor portions of them could be observed, indicating a complete film biodegradation. This result
455 suggests that the *in-vivo* degradation process of all the three matrices was suitable for the complete
456 repair and regeneration of the injured skin tissue.



457

458 **Figure 9.** (A) *In vivo* wound healing model (murine burn/excisional model); (B) Photographical
 459 representation of wound healing in rats exposed to treatments on days (0, 3, 7, 14 and 18 days);
 460 (C) H&E (left panel) and PSR (central panel – with bright field images; right panel – with polarized
 461 light) sections of lesion treated with saline solution as negative control, healthy skin, lesion treated
 462 with WPI film and lesion treated with WPZ film. Original magnification: Original magnification:
 463 5×. Each micrograph frame has a width of 1780 μm. Orange-to-red collagen fibers are visible in
 464 right panel. (D) Wound area retraction % vs. time obtained during the treatments (mean values ±
 465 S.E.; n = 4).

466 4. CONCLUSIONS

467 Wound healing and antimicrobial resistance are serious issues for global health. Elderly
 468 population is at high risk of developing chronic wounds due to the high prevalence of chronic

469 conditions, such as cardiovascular disease and diabetes, impaired mobility, incontinence, low
470 weight, poor nutritional status, and cognitive impairment. Such chronic wounds are generally
471 susceptible to hard-to-treat infections. Finding new wound dressings is imperative to alleviate
472 these burdens and to improve the quality of life of millions of people. Since whey proteins are by-
473 products of the dairy industry with well-known beneficial properties, they can be considered a
474 valuable biomaterial candidate for the development of affordable and sustainable systems for
475 tissue regeneration. Given these premises, the present work aimed: i) to prove the potential of WPI
476 films as novel wound dressings; ii) to evaluate if the addition of nZnO in the whey proteins matrix
477 provides antibacterial properties; iii) to investigate if the combination of WPI with nZnO in WPZ
478 films synergically enhances wound healing. To achieve these aims, WPI and WPZ films have been
479 subjected to a deep functional and biopharmaceutical characterization that showed how these films
480 have wettability, hydration, degradation and rheological properties functional to their use as wound
481 dressings. Such films were also characterized by cytocompatibility, fibroblast proliferation-
482 enhancing properties and antibacterial activity. *In-vivo* studies confirmed their effectiveness to
483 promote wound healing.

484 Further studies will be focused on the production of wound dressings based on novel
485 biomaterials, consisting in complexes between whey proteins and polysaccharides, characterized
486 by optimal biodegradability, ease workability and improved wound healing potential. Continuous
487 manufacturing procedures, such as electrospinning, spray-drying and 3D-printing, will be
488 considered to obtain fibrous membranes, microparticles and films, respectively, with a very low
489 environmental impact.

490

491 **ACKNOWLEDGEMENT**

492 This research was partially supported by EU funding within the NextGenerationEU-
493 MUR PNRR Extended Partnership initiative on Emerging Infectious Diseases (PE13 INF-ACT-
494 F13C22001220007-PE00000007).

495 **AUTHOR INFORMATION**

496 **Corresponding Author**

497 **Silvia Rossi**

498 Department of Drug Sciences, University of Pavia, Via Taramelli 12, Pavia, 27100, Italy,

499 Tel +39 0382987357, Fax +39 0382422975, Email silvia.rossi@unipv.it

500 **Barbara Onida**

501 Department of Applied Science and Technology, Politecnico di Torino, Corso Duca degli
502 Abruzzi 24, Torino, 10129, Italy,

503 Tel +39 0110904631, Email barbara.onida@polito.it

504 **Author Contributions**

505 The manuscript was written through contributions of all authors. All authors have given approval
506 to the final version of the manuscript.

507 **ABBREVIATIONS**

508 WPI, Whey Protein Isolate; nZnO, nanostructured ZnO; ROS, Reactive Oxygen Species; WCA,
509 Water Contact Angle; PBS, Phosphate Buffer Solution; SR, Swelling Ratio; LVR, Linear
510 Viscoelastic Region; R, Residual mass; OD, Optical Density; CFU, Colony Forming Units; ME,
511 Microbial Effect; NHDF, Normal Human Dermal Fibroblasts; H&E, Hematoxylin and Eosin;
512 PSR, Picrosirius Red.

513 **REFERENCES**

- 514 (1) M. Olsson, K. Järbrink, U. Divakar, R. Bajpai, Z. Upton, A. Schmidtchen, J Car, The
515 humanistic and economic burden of chronic wounds: A systematic review. *Wound Repair*
516 *Regen.* 27 (2019) 114–125. DOI: 10.1111/wrr.12683
- 517 (2) C. K. Sen, *Human Wound and Its Burden: Updated 2020 Compendium of Estimates*, *Adv.*
518 *Wound Care (New Rochelle)* 10 (2021) 281-292. DOI: 10.1089/wound.2021.0026
- 519 (3) K. Las Heras, M. Igartua, E. Santos-Vizcaino, R. M. Hernandez, *Chronic wounds: Current*
520 *status, available strategies and emerging therapeutic solutions*, *J. Control Release* 328 (2020)
521 532-550. DOI: 10.1016/j.jconrel.2020.09.039
- 522 (4) D. Li, W. Cao, Q. Zhou, X. Wu, X. Song, H. Qin, *COVID-19 and primary wound healing:*
523 *A new insights and advance*, *Int. Wound J.* (2023). DOI: 10.1111/iwj.14324
- 524 (5) J. Balikji, P. Kiani, P. A. Hendriksen, M. M. Hoogbergen, J. Garssen, J. C. Verster, *Impaired*
525 *wound healing is associated with poorer mood and reduced perceived immune fitness during*
526 *the COVID-19 pandemic: A retrospective survey*, *Health Sci. Rep.* 5 (2022) e764. DOI:
527 10.1002/hsr.2.764.
- 528 (6) M.A. Abushaheen, Muzahed, A.J. Fatani, M. Alosaimi, W. Mansy, M. George, S. Acharya,
529 S. Rathod, D.D. Divakar, C. Jhugroo, S. Vellappally, A.A. Khan, J. Shaik, P. Jhugroo,
530 *Antimicrobial resistance, mechanisms and its clinical significance*, *Dis. Mon.* 66 (2020)
531 100971. DOI: 10.1016/j.disamonth.2020.100971
- 532 (7) E. Rezvani Ghomi, S. Khalili, S. Nouri Khorasani, R. Esmaeely Neisiany, S. Ramakrishna,
533 *Wound dressings: Current advances and future directions*, *J. Appl. Polym. Sci.* 136 (2019)
534 47738. DOI: 10.1002/APP.47738

- 535 (8) R. Laurano, M. Boffito, G. Ciardelli, V. Chiono, Wound dressing products: A translational
536 investigation from the bench to the market, *Eng. Regen.* 3 (2022) 182–200. DOI:
537 10.1016/j.engreg.2022.04.002
- 538 (9) S. Sharifi, M. J. Hajipour, L. Gould, M. Mahmoudi, Nanomedicine in Healing Chronic
539 Wounds: Opportunities and Challenges, *Mol. Pharm.* 18 (2021) 550-575. DOI:
540 10.1021/acs.molpharmaceut.0c00346
- 541 (10) A. Pormohammad, N.K. Monych, S. Ghosh, D.L. Turner, R.J. Turner, Nanomaterials in
542 Wound Healing and Infection Control. *Antibiotics.* 10 (2021) 473. DOI:
543 10.3390/ANTIBIOTICS10050473
- 544 (11) P.K. Mishra, H. Mishra, A. Ekielski, S. Talegaonkar, B. Vaidya, Zinc oxide nanoparticles:
545 a promising nanomaterial for biomedical applications, *Drug Discov. Today.* 22 (2017) 1825–
546 1834. DOI: 10.1016/J.DRUDIS.2017.08.006
- 547 (12) A. Sirelkhatim, S. Mahmud, A. Seeni, N. H. M. Kaus, L. C. Ann, S. K. M. Bakhori, H.
548 Hasan, D. Mohamad, Review on Zinc Oxide Nanoparticles: Antibacterial Activity and
549 Toxicity Mechanism, *Nanomicro. Lett.* 7 (2015) 219-242. DOI:10.1007/s40820-015-0040-
550 x.
- 551 (13) P. Pino, F. Bosco, C. Mollea, B. Onida, Antimicrobial Nano-Zinc Oxide Biocomposites
552 for Wound Healing Applications: A Review, *Pharmaceutics* 15 (2023) 970. DOI:
553 10.3390/pharmaceutics15030970.
- 554 (14) A.B.G. Lansdown, U. Mirastschijski, N. Stubbs, E. Scanlon, M.S. Ågren, Zinc in wound
555 healing: Theoretical, experimental, and clinical aspects, *Wound Repair Regen.* 15 (2007) 2–
556 16. DOI: 10.1111/J.1524-475X.2006.00179.X

- 557 (15) S. Sruthi, J. Ashtami, P.V. Mohanan, Biomedical application and hidden toxicity of Zinc
558 oxide nanoparticles, *Mater. Today Chem.* 10 (2018) 175-186. DOI:
559 10.1016/j.mtchem.2018.09.008
- 560 (16) S. Karki, M. B. Gohain, D. Yadav, P. G. Ingole, Nanocomposite and bio-nanocomposite
561 polymeric materials/membranes development in energy and medical sector: A review, *Int. J.*
562 *Biol. Macromol.* 193 (2021) 2121-2139. DOI: 10.1016/j.ijbiomac.2021.11.044.
- 563 (17) E. Zandona, M. Blazic, A.R. Jambrak, Whey Utilization: Sustainable Uses and
564 Environmental Approach, *Food Technol. Biotechnol.* 59 (2021), 147-161. DOI:
565 10.17113/ftb.59.02.21.6968
- 566 (18) R. Mehra, H. Kumar, N. Kumar, S. Ranvir, A. Jana, H.S. Buttar, I.G. Telessy, C.G.
567 Awuchi, C.O.R. Okpala, M. Korzeniowska, R.F.P. Guiné, Whey proteins processing and
568 emergent derivatives: An insight perspective from constituents, bioactivities, functionalities
569 to therapeutic applications, *J. Funct. Foods.* 87 (2021) 104760. DOI:
570 10.1016/J.JFF.2021.104760
- 571 (19) E. Arribas-López, N. Zand, O. Ojo, M.J. Snowden, T. Kochhar, The Effect of Amino Acids
572 on Wound Healing: A Systematic Review and Meta-Analysis on Arginine and Glutamine,
573 *Nutrients* 13 (2021), 2498. DOI: 10.3390/nu13082498.
- 574 (20) K. Khwaldia, C. Ferez, S. Banon, S. Desobry, J. Hardy, Milk proteins for edible films and
575 coatings. *Crit. Rev. Food Sci. Nutr.* 44 (2004) 239–251. DOI: 10.1080/10408690490464906
- 576 (21) H. Chen, J. Wang, Y. Cheng, C. Wang, H. Liu, H. Bian, Y. Pan, J. Sun, W. Han,
577 Application of Protein-Based Films and Coatings for Food Packaging: A Review, *Polymers*
578 (Basel) 11 (2019) 2039. DOI: 10.3390/polym11122039.

- 579 (22) S. Kandasamy, J. Yoo, J. Yun, H.B. Kang, K.H. Seol, H.W. Kim, J.S. Ham, Application
580 of Whey Protein-Based Edible Films and Coatings in Food Industries: An Updated
581 Overview, *Coatings*. 11 (2021) 1056. DOI: 10.3390/coatings11091056
- 582 (23) H. Ebaid, A. Salem, A. Sayed, A. Metwalli, Whey protein enhances normal inflammatory
583 responses during cutaneous wound healing in diabetic rats, *Lipids Health Dis*. 10 (2011) 235.
584 DOI: 10.1186/1476-511X-10-235.
- 585 (24) O. Garraud, W. N. Hozzein, G. Badr, Wound healing: time to look for intelligent, 'natural'
586 immunological approaches?, *BMC Immunol*. 18 (2017) 23. DOI: 10.1186/s12865-017-
587 0207-y.
- 588 (25) P. Pino, S. Ronchetti, C. Mollea, M. Sangermano, B. Onida, F. Bosco, Whey Proteins–
589 Zinc Oxide Bionanocomposite as Antibacterial Films. *Pharmaceutics*, 13 (2021) 1426. DOI:
590 10.3390/PHARMACEUTICS13091426
- 591 (26) H. Chopra, S. Bibi, S. Kumar, S.K. Muhammad, P. Kumar, I. Singh, Preparation and
592 Evaluation of Chitosan/PVA Based Hydrogel Films Loaded with Honey for Wound Healing
593 Application, *Gels*. 8 (2022) 111. DOI: 10.3390/gels8020111
- 594 (27) C. Ransy, C. Vaz, A. Lombès, F. Bouillaud, Use of H₂O₂ to Cause Oxidative Stress, the
595 Catalase Issue, *Int. J. Mol. Sci*. 21 (2020) 9149. DOI: 10.3390/ijms21239149
- 596 (28) N. J. Anthis, G. M. Clore, Sequence-specific determination of protein and peptide
597 concentrations by absorbance at 205 nm, *Protein Sci*. 22 (2013) 851-858. DOI:
598 10.1002/pro.2253. Epub 2013 Apr 29.

- 599 (29) A.P. Fraise, J. Maillard, S. Sattar, (Eds.), Russell, Hugo and Ayliffe's Principles and
600 Practice of Disinfection, Preservation and Sterilization. 5th Edition, Wiley-Blackwell
601 Publishing, 2012
- 602 (30) P. Grisoli, L. De Vita, C. Milanese, A. Taglietti, Y. Diaz Fernandez, M. Bouzin, L.
603 D'Alfonso, L. Sironi, L., S. Rossi, B. Vigani, P. Sperandeo, A. Polissi, P. Pallavicini, PVA
604 Films with Mixed Silver Nanoparticles and Gold Nanostars for Intrinsic and Photothermal
605 Antibacterial Action, *Nanomaterials* (Basel). 11 (2021) 1387. DOI: 10.3390/nano11061387
- 606 (31) R. Podgórski, M. Wojasiński, T. Ciach, Nanofibrous materials affect the reaction of
607 cytotoxicity assays, *Sci. Rep.* 12 (2022) 9047. DOI: 10.1038/s41598-022-13002-w
- 608 (32) M. Tenci, S. Rossi, M.C. Bonferoni, G. Sandri, C. Boselli, A. Di Lorenzo, M. Daglia, A.
609 Icaro Cornaglia, L. Gioglio, C. Perotti, C. Caramella, F. Ferrari, Particulate systems based
610 on pectin/chitosan association for the delivery of manuka honey components and platelet
611 lysate in chronic skin ulcers, *Int. J. Pharm.* 509 (2016) 59-70.
612 DOI:10.1016/j.ijpharm.2016.05.035
- 613 (33) L.C. Junqueira, W. Cossermelli, R. Brentani, Differential staining of collagens type I, II
614 and III by Sirius Red and polarization microscopy, *Arch. Histol. Jpn.* 41 (1978) 267-74.
615 DOI: 10.1679/aohc1950.41.267
- 616 (34) R. Lattouf, R. Younes, R., D. Lutomski, N. Naaman, G. Godeau, K. Senni, S.
617 Changotade, Picosirius red staining: a useful tool to appraise collagen networks in normal
618 and pathological tissues, *J. Histochem. Cytochem.* 62 (2014) 751-758. DOI:
619 10.1369/0022155414545787

- 620 (35) O.B. Karaca, C.A. Oluk, T. Taşpinar, M. Güven, New Concept in Packaging: Milk
621 Protein Edible Films. In: A. Malik, Z. Erginkaya, H. Erten (Eds), Health and Safety
622 Aspects of Food Processing Technologies. Springer, Cham. 2019. DOI: 10.1007/978-3-
623 030-24903-8_19
- 624 (36) J.M. Kassem, Future Challenges of Whey Proteins, *Int. J. Dairy Sci.* 10 (2015) 139–59.
625 DOI:10.3923/IJDS.2015.139.159
- 626 (37) A.A. Hemmati, A. Larki-Harchegani, S. Shabib, A. Jalali, A. Rezaei, G. Housmand,
627 Wound healing property of milk in full thickness wound model of rabbit, *Int. J. Surg.* 54
628 (2018) 133-140. DOI: 10.1016/j.ijssu.2018.04.030
- 629 (38) M.M. Agwa, S. Sabra, N.A. Atwa, H.A. Dahdooh, R.M. Lithy, H. Elmotasem, Potential
630 of frankincense essential oil-loaded whey protein nanoparticles embedded in frankincense
631 resin as a wound healing film based on green technology, *J. Drug Deliv. Sci. Technol.* 71
632 (2022) 103291. DOI: 10.1016/J.JDDST.2022.103291
- 633 (39) N. Melnikova, A. Knyazev, V. Nikolskiy, P. Peretyagin, K. Belyaeva, N. Nazarova, E.
634 Liyaskina, D. Malygina, V. Revin, Wound Healing Composite Materials of Bacterial
635 Cellulose and Zinc Oxide Nanoparticles with Immobilized Betulin Diphosphate,
636 *Nanomaterials (Basel)*. 11 (2021) 713. DOI: 10.3390/nano11030713
- 637 (40) D. Salarbashi, S. A. Mortazavi, M. S. Noghabi, B. S. F. Bazzaz, N. Sedaghat, M.
638 Ramezani, I. Shahabi-Ghahfarrokhi, Development of new active packaging film made from
639 a soluble soybean polysaccharide incorporating ZnO nanoparticles, *Carbohydr. Polym.* 140
640 (2016) 220-227. DOI: 10.1016/j.carbpol.2015.12.043

- 641 (41) P. Kanmani, J.-W. Rhim, Properties and characterization of bionanocomposite films
642 prepared with various biopolymers and ZnO nanoparticles, *Carbohydr. Polym.* 106 (2014)
643 190-199. DOI: 10.1016/j.carbpol.2014.02.007.
- 644 (42) J. A. A. Abdullah, M. Jimenez-Rosado, A. Guerrero, A. Romero, Biopolymer-Based
645 Films Reinforced with Green Synthesized Zinc Oxide Nanoparticles, *Polymers (Basel)* 14
646 (2022) 5202. DOI: 10.3390/polym14235202.
- 647 (43) P. Kanmani, J.W. Rhim, Properties and characterization of bionanocomposite films
648 prepared with various biopolymers and ZnO nanoparticles, *Carbohydr. Polym.* 106 (2014)
649 190-199. DOI: 10.1016/j.carbpol.2014.02.007
- 650 (44) M.T. Khorasani, A. Joorabloo, A. Moghaddam, H. Shamsi, Z. Mansoori Moghadam,
651 Incorporation of ZnO nanoparticles into heparinised polyvinyl alcohol/chitosan hydrogels
652 for wound dressing application, *Int. J. Biol. Macromol.* 114 (2018) 1203-1215. DOI:
653 10.1016/j.ijbiomac.2018.04.010
- 654 (45) S. Roy, J.W. Rhim, Carrageenan-Based Antimicrobial Bionanocomposite Films
655 Incorporated with ZnO Nanoparticles Stabilized by Melanin, *Food Hydrocoll.* 90 (2019)
656 500–507. DOI:10.1016/J.FOODHYD.2018.12.056
- 657 (46) Q. Du, P. Zhou, Y. Pan, X. Qu, L. Liu, H. Yu, J. Hou, Influence of hydrophobicity and
658 roughness on the wetting and flow resistance of water droplets on solid surface: A many-
659 body dissipative particle dynamics study, *Chem. Eng. Sci.* 249 (2022) 117327. DOI:
660 10.1016/j.ces.2021.117327

- 661 (47) X. Liu, T. Lin, J. Fang, G. Yao, H. Zhao, M. Dodson, X. Wang, In vivo wound healing
662 and antibacterial performances of electrospun nanofibre membranes, *J. Biomed. Mater.*
663 *Res. A.* 94 (2010) 499-508. DOI:10.1002/jbm.a.32718
- 664 (48) K. Kalantari, M. Ebrahim, B. Saleh, P. Soltantabar, T.J. Webster, Chitosan/PVA
665 Hydrogels Incorporated with Green Synthesized Cerium Oxide Nanoparticles for Wound
666 Healing Applications, *Eur. Polym. J.* 134 (2020) 109853.
667 DOI:10.1016/J.EURPOLYMJ.2020.109853
- 668 (49) D. George, P.U. Maheswari, K.M.M.S. Begum, Chitosan-cellulose hydrogel conjugated
669 with L-histidine and zinc oxide nanoparticles for sustained drug delivery: Kinetics and in-
670 vitro biological studies, *Carbohydr. Polym.* 236 (2020) 116101. DOI:
671 10.1016/j.carbpol.2020.116101
- 672 (50) M.E. Villanueva, M.L. Cuestas, C.J. Pérez, V. Campo Dall'Orto, G.J. Copello, Smart
673 release of antimicrobial ZnO nanoplates from a pH-responsive keratin hydrogel, *J. Colloid.*
674 *Interface Sci.* 536 (2019) 372-380. DOI: 10.1016/j.jcis.2018.10.067
- 675 (51) M. Mori, S. Rossi, F. Ferrari, M.C. Bonferoni, G. Sandri, T. Chlapanidas, M.L. Torre, C.
676 Caramella, Sponge-Like Dressings Based on the Association of Chitosan and Sericin for
677 the Treatment of Chronic Skin Ulcers. I. Design of Experiments-Assisted Development, *J.*
678 *Pharm. Sci.* 105 (2016) 1180-1187. DOI: 10.1016/j.xphs.2015.11.047
- 679 (52) M.M. Gonçalves, J. Carneiro, B. Justus, J.T. Espinoza, J. M. Budel, P.V. Farago, J.P.D.
680 Paula, Preparation and Characterization of a Novel Antimicrobial Film Dressing for
681 Wound Healing Application, *Braz. J. Pharm. Sci.* 56 (2021). DOI:10.1590/S2175-
682 97902020000118784

- 683 (53) P.I. Morgado, A. Aguiar-Ricardo, I.J. Correia, Asymmetric Membranes as Ideal Wound
684 Dressings: An Overview on Production Methods, Structure, Properties and Performance
685 Relationship, *J. Membr. Sci.* 490 (2015) 139–151. DOI:10.1016/J.MEMSCI.2015.04.064
- 686 (54) W.C. Lin, C.C. Lien, H.J. Yeh, C.M. Yu, S.H. Hsu, Bacterial cellulose and bacterial
687 cellulose-chitosan membranes for wound dressing applications, *Carbohydr. Polym.* 94
688 (2013) 603-611. DOI: 10.1016/j.carbpol.2013.01.076
- 689 (55) B. Vigani, C. Valentino, V. Cavalloro, L. Catenacci, M. Sorrenti, G. Sandri, M.C.
690 Bonferoni, C. Bozzi, S. Collina, S. Rossi, F. Ferrari, Gellan-Based Composite System as a
691 Potential Tool for the Treatment of Nervous Tissue Injuries: Cross-Linked Electrospun
692 Nanofibers Embedded in a RC-33-Loaded Freeze-Dried Matrix, *Pharmaceutics*. 13 (2021)
693 164. DOI: 10.3390/pharmaceutics13020164
- 694 (56) S. Keshavarzi, A. Babaei, A. Goudarzi, A. Shakeri, ZnO nanoparticles as chain elasticity
695 reducer and structural elasticity enhancer: Correlating the degrading role and localization
696 of ZnO with the morphological and mechanical properties of PLA/PP/ZnO nanocomposite,
697 *Polym. Adv. Technol.* 30 (2019) 1083–1095. DOI: 10.1002/pat.4542
- 698 (57) M. Schäfer, S. Werner, Oxidative stress in normal and impaired wound repair,
699 *Pharmacol. Res.* 58 (2008) 165-171. DOI: 10.1016/j.phrs.2008.06.004
- 700 (58) B. Vigani, S. Rossi, G. Sandri, M.C. Bonferoni, M. Rui, S. Collina, F. Fagiani, C. Lanni,
701 F. Ferrari, Dual-Functioning Scaffolds for the Treatment of Spinal Cord Injury: Alginate
702 Nanofibers Loaded with the Sigma 1 Receptor (S1R) Agonist RC-33 in Chitosan Films,
703 *Mar. Drugs*. 18 (2019) 21. DOI: 10.3390/md18010021

- 704 (59) K. Khwaldia, S. Banon, S. Desobry, J. Hardy, Mechanical and barrier properties of
705 sodium caseinate–anhydrous milk fat edible films, *JFST*. 39 (2004) 403-411. DOI:
706 10.1111/j.1365-2621.2004.00797.x
- 707 (60) A.K. Ghosh, B. Prasun, Polysaccharide-Protein Interactions and Their Relevance in Food
708 Colloids. In: D.N. Karunaratne, (Ed), *The Complex World of Polysaccharides*. IntechOpen,
709 2012. DOI: 10.5772/50561
- 710 (61) E. Yuan, M. Zhou, S. Nie, J. Ren, Interaction mechanism between ZnO nanoparticles-
711 whey protein and its effect on toxicity in GES-1 cells, *J. Food Sci.* 87 (2022) 2417-2426.
712 DOI: 10.1111/1750-3841.16193.
- 713 (62) W. Zhang, M. A. Sani, Z. Zhang, D. J. Clements, S. M. Jafari, High performance
714 biopolymeric packaging films containing zinc oxide nanoparticles for fresh food
715 preservation: A review, *Int. J. Biol. Macromol.* 230 (2023) 123188. DOI:
716 10.1016/j.ijbiomac.2023.123188.
- 717 (63) P.J.P. Espitia, N.F.F. Soares, J.S.R. Coimbra, N.J. de Andrade, R.S. Cruz, E.A.A.
718 Medeiros, Zinc Oxide Nanoparticles: Synthesis, Antimicrobial Activity and Food
719 Packaging Applications, *Food Bioprocess. Technol.* 5 (2012) 1447–1464. DOI:
720 10.1007/s11947-012-0797-6
- 721 (64) M. Gupta, V.K. Mahajan, K.S. Mehta, P.S. Chauhan, Zinc therapy in dermatology: a
722 review, *Dermatol. Res. Pract.* (2014) 709152. DOI: 10.1155/2014/709152
- 723 (65) I. Wessels, M. Maywald, L. Rink, Zinc as a Gatekeeper of Immune Function. *Nutrients*. 9
724 (2017) 1286. DOI: 10.3390/nu9121286

725 (66) A.J. Singer, R.A.F. Clark, *Cutaneous Wound Healing*. Edited by Franklin H. Epstein 341
726 (1999), 738–46. DOI:10.1056/NEJM199909023411006.